

Improving the Thermal Stability of Top-Emitting Organic Light-Emitting Diodes by Modification of the Anode Interface

Yali Deng, Changmin Keum, Sabina Hillebrandt, Caroline Murawski, and Malte C. Gather*

Top-emitting organic light-emitting diodes (OLEDs) are of interest for numerous applications, in particular for displays with high fill factors. To maximize efficiency and luminance, molecular p-doping of the hole transport layer (p-HTL) and a highly reflective anode contact, for example, made from silver, are used. Atomic layer deposition (ALD) is attractive for thin film encapsulation of OLEDs but generally requires a minimum process temperature of 80 °C. Here it is reported that the interface between the p-HTL and the silver anode of top-emitting OLEDs degrades during an 80 °C ALD encapsulation process, causing an over fourfold reduction in OLED current and luminance. To understand the underlying mechanism of device degradation, single charge carrier devices are investigated before and after annealing. A spectroscopic study of p-HTLs indicates that degradation is due to the interaction between diffusing silver ions and the p-type molecular dopant. To improve the stability of the interface, either an ultrathin MoO₃ buffer layer or a bilayer HTL is inserted at the anode/organic interface. Both approaches effectively suppress degradation. This work shows a route to successful encapsulation of top-emitting OLEDs using ALD without sacrificing device performance.

1. Introduction

Organic light-emitting diodes (OLEDs) have been extensively studied over the past few decades and have now become an established technology for information displays. OLEDs offer a number of attractive properties, such as small size, light weight, wide viewing angle, color tunability, fast response time, and compatibility with flexible substrates.^[1,2] Depending on the direction of light emission, one can distinguish two principal OLED architectures. In bottom-emitting OLEDs, light is emitted through a transparent glass or plastic substrate whereas in top-emitting devices light is emitted away from the substrate thus allowing the use of opaque substrates.^[3,4] The top-emitting configuration is beneficial, for example, in display applications, in particular where high resolution is required, as it allows the use of non-transparent backplane technology for active matrix driving of OLEDs. Stacking

the OLED on top of the pixel transistors forming the backplane allows high fill factors and avoids having to divide up the area of each pixel between transistors and OLED. An example where the top-emitting configuration is essential is when OLEDs are deposited on silicon-based complementary metal oxide semiconductor (CMOS) backplanes. Combining OLEDs with such CMOS drivers allows the realization of microdisplays for near-to-eye applications.^[5-7] In addition, this combination is of interest for bioimplants and biomedical sensors to realize individually controllable OLED pixels with dimensions comparable to single cells, which is useful for optical manipulation and interrogation of biological activity at the cellular level.^[8,9]


To enable efficient and robust top-emitting OLEDs, substantial research has gone into developing suitable top electrodes that provide high optical transmission and high electrical conductivity and that can be deposited onto sensitive organic layers without degrading the device.^[10] Promising approaches include ultrathin metallic top electrodes,^[11,12] low-energy deposition of transparent conductive oxides,^[13,14] and the use of nanotube networks.^[15,16] On the other hand, the bottom electrode needs to be highly reflective to realize efficient top-emitting OLEDs. Silver provides the highest reflectance across most of the visible

Y. Deng, Dr. C. Keum, Dr. S. Hillebrandt, Dr. C. Murawski,
Prof. M. C. Gather
Organic Semiconductor Centre
SUPA

School of Physics and Astronomy
University of St Andrews
St Andrews KY16 9SS, UK
E-mail: mcg6@st-andrews.ac.uk

Dr. C. Murawski
Kurt-Schwabe-Institut für Mess- und Sensortechnik Meinsberg e.V.
Kurt-Schwabe-Str. 4, 04736 Waldheim, Germany

Prof. M. C. Gather
Centre for NanoBioPhotonics
Department of Chemistry
University of Cologne
Greinstr. 4–6, 50939 Köln, Germany

 The ORCID identification number(s) for the author(s) of this article can be found under <https://doi.org/10.1002/adom.202001642>.

© 2020 The Authors. Advanced Optical Materials published by Wiley-VCH GmbH. This is an open access article under the terms of the Creative Commons Attribution License, which permits use, distribution and reproduction in any medium, provided the original work is properly cited.

DOI: 10.1002/adom.202001642

spectrum among the available metals and offers good electrical conductivity. However, surface roughness needs to be managed to avoid poor yield and large leakage currents.^[17–19] In addition, if metallic electrodes are used on both sides of the device, the OLED emission is often governed by microcavity effects which need to be carefully controlled to obtain the desired efficiency and spectral characteristics.^[20–22] P-type doping of the hole transport layer (p-HTL) and n-type doping of the electron transport layer (n-ETL), which is widely used in state-of-the-art OLEDs to reduce operating voltage,^[23,24] allows fine-tuning of the thickness of the transport layers without compromising conductivity and thus permits controlling microcavity effects.

Another issue that requires attention in top-emitting OLEDs is environmental stability and device degradation.^[25] Due to the thin top electrode of these devices, water and oxygen can attack the sensitive organic layers even more readily than in conventional bottom-emitting OLEDs. Therefore, a highly protective encapsulation technique is generally required, and robust thin film encapsulation (TFE) is essential to realize flexible devices. Process temperature is a key consideration when choosing the appropriate method for depositing TFE as excessive temperatures cause crystallization of organic materials with low glass transition temperatures (T_g).^[26,27] Additionally, thermal diffusion of small molecules or metal ions can lead to degradation, for example, through the formation of nonradiative recombination centers.^[28–30] Atomic layer deposition (ALD) can be operated at low working temperatures (down to 80 °C) when compared with other encapsulation technologies, such as chemical vapor deposition.^[31] Indeed, ALD has been shown to offer TFE with suitable characteristics in many cases.^[32–34] However, it has not been possible to obtain efficient TFE, by ALD or other means, for top-emitting OLEDs that use a p-HTL and a silver bottom electrode, even though this combination is highly desirable to achieve optimal device performance.

In this work, we report an effective method to suppress device degradation during TFE in top-emitting OLEDs by modifying the silver/HTL interface. Our work starts from the observation that even when using materials with sufficiently high T_g , the current density and luminance of top-emitting OLEDs decrease significantly when a thermal process is applied that involves heating to 80 °C, such as TFE deposition. To investigate the underlying

mechanism, the current density–voltage (j/V) characteristics of hole only devices (p–i–p) and electron only devices (n–i–n) were analyzed after annealing at 80 °C for different durations. Annealing did not have a substantial effect on the n–i–n device but caused a dramatic loss in current density for the p–i–p device. This led us to identify the interface between the silver bottom electrode and the p-HTL as the weak point in the structure. A spectroscopic study confirmed that at elevated temperature silver ions interact with the HTL in a way that reduces the efficiency of p-type doping. To stabilize the silver/HTL interface, we either inserted an ultrathin MoO₃ buffer layer or used a bilayer HTL. Both approaches improved thermal stability at elevated temperatures, allowing to successfully apply ALD-based TFE to top-emitting p–i–n OLEDs without sacrificing device performance.

2. Results and Discussion

2.1. Device Degradation during Atomic Layer Deposition Encapsulation

Figure 1a shows the device structure of the blue top-emitting p–i–n OLEDs used in this study. The devices had a thick (80 nm) silver bottom electrode and a thin (20 nm) silver top electrode. For protection and optical microcavity adjustment, a 40 nm-thick organic capping layer was deposited subsequent to the top electrode.^[35] All devices have an HTL of 2,2',7,7'-tetrakis(N,N'-di-p-methylphenylamino)-9,9'-spirobifluorene (Spiro-TTB), p-doped with 2,2'-(perfluoronaphthalene-2,6-diylidene)dimalononitrile (F6-TCNNQ), and an ETL, n-doped with Cs. ETL materials with different T_g were compared, specifically 4,7-diphenyl-1,10-phenanthroline (BPhen), 2,9-dinaphthalen-2-yl-4,7-diphenyl-1,10-phenanthroline (NBPhen), and 1,3,5-Tris(1-phenyl-1Hbenzimidazol-2-yl)benzene (TPBi). The thickness of the HTL and ETL was optimized for maximum light out-coupling efficiency using optical modeling (Figure S1a,b, Supporting Information). We found that the predicted dependence of outcoupling efficiency on HTL thickness was in good agreement with experimental trends in device efficiency (Figure S1c, Supporting Information). As expected for a microcavity OLED, the HTL thickness had a substantial impact on device efficiency.

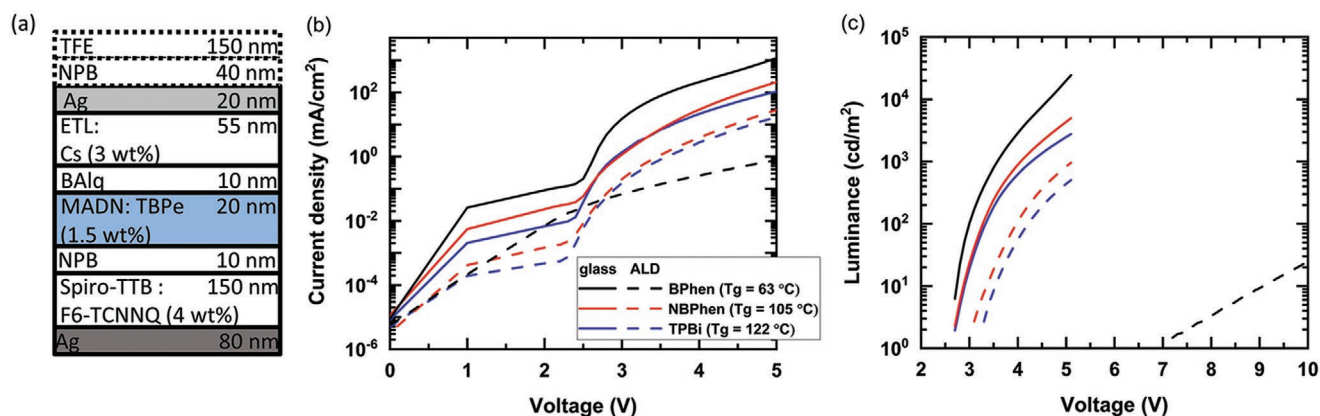


Figure 1. a) Device structure of the blue p–i–n top-emitting OLED used to study and optimize the impact of ALD-based encapsulation at 80 °C. b) Comparison of j/V characteristics for OLEDs encapsulated with a cover glass and OLEDs encapsulated by ALD, testing a set of ETL materials (BPhen, NBPhen, and TPBi) with different glass transition temperatures T_g . c) Comparison of L/V characteristics for same set of OLEDs.

In addition, leakage currents decreased significantly, and device stability improved when adjusting the HTL thickness for the 2nd rather than the 1st order cavity mode (Figure S1d, Supporting Information). Hence, devices designed for the 2nd order cavity mode were used throughout the rest of this study.

Immediately after fabrication, our OLEDs were encapsulated either with conventional cover glasses with embedded getters or by depositing alternating layers of Al₂O₃ and ZrO₂ (total thickness, 150 nm) in an ALD reactor. Figure 1b,c compares the current density–voltage–luminance (*j*VL) characteristics of the different OLEDs. Amongst the devices with glass encapsulation, the OLED using BPhen as an ETL exhibited the best performance in terms of current density and luminance, achieving 1200 mA cm⁻² and 20 000 cd m⁻² at 5 V, respectively. OLEDs with NBPhen and TPBi showed lower current density and luminance but comparable external quantum efficiency (EQE, Figure S2, Supporting Information). We attribute this difference to the high charge mobility and deep lowest unoccupied molecular orbital level of BPhen.^[36,37] However, when instead using ALD encapsulation, which involves heating the devices to a temperature of 80 °C for several hours, the current density in the BPhen device became dramatically lower (0.8 mA cm⁻² at 5 V) and no detectable emission was observed up to a voltage of 7 V. This large difference is due to the low *T*_g of BPhen (63 °C), which leads to crystallization of the ETL during processes requiring elevated temperatures.

This problem can be solved by increasing the Cs doping level of BPhen.^[38] Alternatively, one can select materials with higher *T*_g, however, at the cost of reduced current density and luminance compared to BPhen.^[39,40] For devices with an ETL of NBPhen (*T*_g = 105 °C) and TPBi (*T*_g = 122 °C), the difference between glass and ALD encapsulation was indeed much smaller than for the BPhen case. However, even though the *T*_g of these materials is well above the ALD process temperature, both current density and luminance of the OLED encapsulated by ALD were still significantly reduced relative to conventional glass encapsulation (from 210 mA cm⁻², 4300 cd m⁻² at 5 V to 30 mA cm⁻², 830 cd m⁻² for NBPhen and from 110 mA cm⁻², 2500 cd m⁻² at 5 V to 17 mA cm⁻², 440 cd m⁻² for TPBi). Thus, for the top-emitting OLEDs studied here, degradation clearly still takes place, even when using morphologically stable materials, indicating that additional factors are at play here. By contrast, there was no appreciable difference between glass and ALD encapsulation for analogous bottom-emitting OLEDs with an NBPhen ETL, an indium tin oxide (ITO) anode, and an aluminum cathode (Figure S3, Supporting Information). Furthermore, we annealed glass-encapsulated devices in the ALD chamber at 80 °C for different lengths of time without running the deposition process, that is, no injection of precursors (Figure S4, Supporting Information). With increasing annealing time the device performance reduced significantly; there was an almost fourfold decrease in current density and luminance at 5 V after 16 h, with the values approaching those observed after ALD encapsulation. This indicates that the elevated temperature during the ALD process is the main cause of the observed degradation.

2.2. Conductivity Test of Single Charge Carrier Devices

To isolate the origin of the degradation during the ALD process, the electrical behavior of single charge carrier devices

was investigated. The n–i–n devices were based on Cs-doped NBPhen, and p–i–p devices used F6-TCNNQ-doped Spiro-TTB. The device structures are illustrated in the top panels of **Figure 2**. Figure 2a,b shows the *j*V curves of n–i–n and p–i–p devices with a thick silver bottom electrode and a thin silver top contact, comparing pristine conditions and annealing at a temperature of 80 °C for different periods of time. The symmetric shape of the *j*V curves indicates efficient charge injection from both contacts. Annealing led to a large decrease in the current density for the p–i–p device while the current density remained virtually unchanged in the n–i–n device. To gain insight into the current injection mechanism in both devices, the *j*V curves in the positive-bias region were replotted on a log–log scale (bottom panels, Figure 2). A nearly linear relationship was observed across the entire voltage range for the n–i–n devices whereas two different slopes were seen for the p–i–p devices—a slope of 1.04 in the low voltage region and a slope >2 in the high voltage region. The linear behavior (slope ≈ 1) in the n–i–n device indicates the formation of Ohmic contacts at the organic/metal interface and that the charge carrier concentration in the doped layer exceeds the concentration of injected charge carriers. The slope >2 in the p–i–p devices suggests a trap-filled space charge limited current process. This slope increases further with annealing time (up to 2.3). We attribute this to surface defects, possibly due to temperature driven diffusion of silver ions, which may form localized interfacial trap states or which could influence the electrical properties in the bulk of the HTL.^[41] Similar diffusion effects are used in creating organic memory devices where metal diffusion leads to the formation of filaments that cause the memory effect, yet in these devices an active electrode (e.g., Ag, Cu) and an inert electrode (e.g., Au, Pt) are paired to form conductive filaments in a dielectric layer sandwiched between the two electrodes.^[42–44]

The influence of the silver contact on degradation is corroborated by the fact that annealing had very little impact on current density in a silver-free p–i–p device in which an ITO layer was used as the bottom electrode and a thick Al layer formed the top electrode (Figure 2c). While Al is not the ideal top contact for a p–i–p device in terms of hole injection, it was chosen over the more noble gold here as the latter may again diffuse into the organic layers. The fact that the *j*V characteristics of the structure are symmetric at negative and positive bias indicates the absence of substantial electron injection from the Al top electrode. In this device the log*j*–log*V* plot revealed three different slopes, which can be interpreted as different stages of charge injection and transport.^[45]

We hypothesized that upon heat exposure diffusing silver ions may interact with the F6-TCNNQ dopant in the Spiro-TTB-based HTL in a manner that reduces its doping efficiency. Therefore, a p–i–p device using MoO₃ as alternative p-dopant was investigated. Transition metal oxides (TMOs) such as MoO₃ have been used as interlayers on the anode side of OLEDs and have been found to enhance hole injection.^[46] TMOs can also serve as dopants for HTLs and as charge generation layers in stacked OLEDs.^[47,48] There was a substantial decrease in current density compared to the p–i–p device using F6-TCNNQ (now reaching 2000 mA cm⁻² only at 4 V, compared to 2 V before), indicating that despite using a higher doping concentration the conductivity of the MoO₃-doped layer is lower (Figure 2d). However, no significant further decrease in current

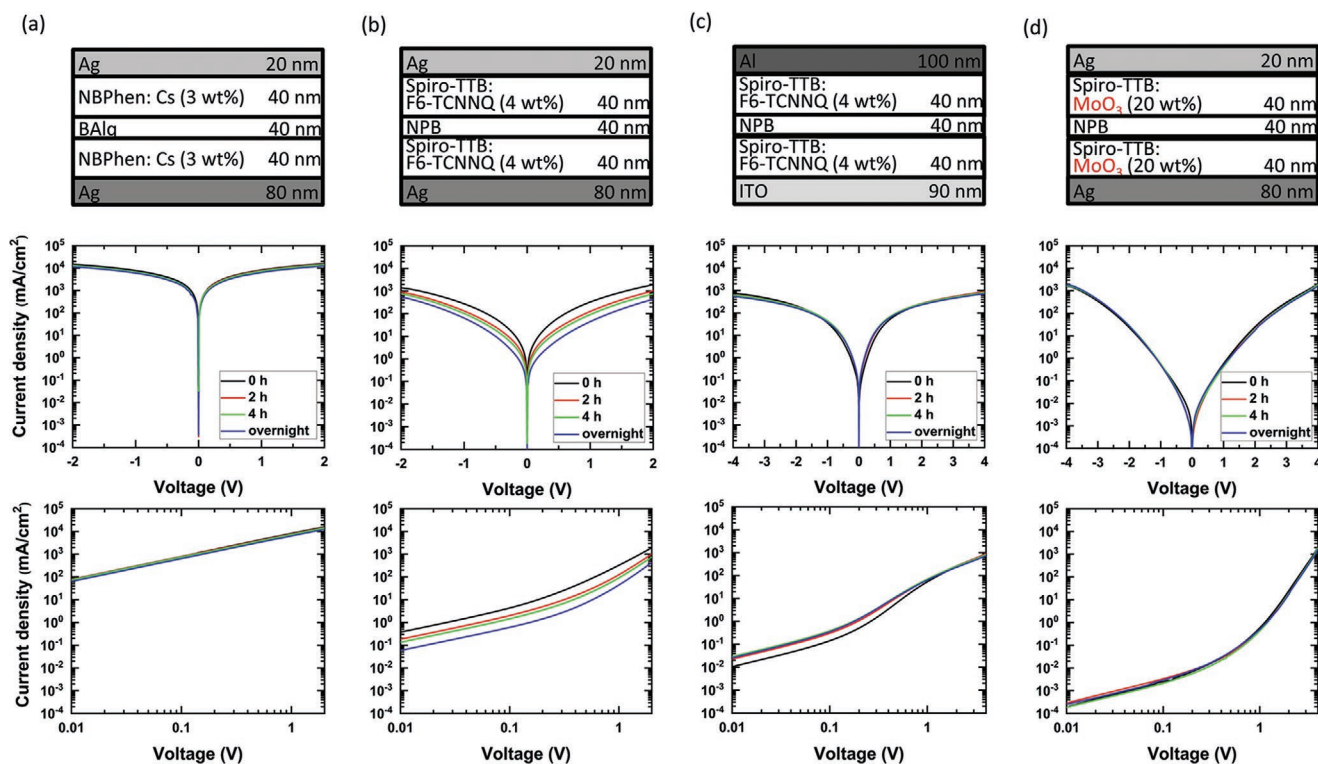


Figure 2. Device structures (top), j/V curves (middle), and $\log j$ - $\log V$ curves (bottom) of pristine single charge carrier devices (0 h) and after annealing at a temperature of 80 °C for 2 h, 4 h, and overnight. a) n-i-n device with a thick layer of silver as bottom and a thin layer of silver as top electrode (similar to the situation in the top-emitting OLEDs discussed before). b) p-i-p device with same electrode configuration as in (a). c) p-i-p device with an ITO bottom and a thick aluminum top electrode. d) p-i-p device using the same electrode configuration as in (b) but with MoO₃ as alternative p-dopant.

density was observed for this device after annealing for different periods of time. This observation supports our picture that silver ions interact with F6-TCNNQ in the HTL when the interface is kept at elevated temperature for extended times and that this reduces doping efficiency in the HTL.

We further verified the involvement of F6-TCNNQ in the process, by comparing complete top-emitting OLEDs with HTLs of undoped Spiro-TTB and of F6-TCNNQ-doped Spiro-TTB (Figure S5, Supporting Information). Although using the undoped HTLs led to much lower overall current density and luminance, its performance was not affected by ALD encapsulation.

2.3. Spectroscopic Study of Silver/p-Hole Transport Layer Interface

Next, we conducted a simple spectroscopic study to better understand the process at the interface between silver and the p-HTL at elevated temperatures. Layers consisting of pure Spiro-TTB, pristine Spiro-TTB doped with F6-TCNNQ, and annealed Spiro-TTB doped with F6-TCNNQ were deposited on thick silver films. **Figure 3** shows the optical reflectance of the different structures. All samples showed high reflectance at visible wavelengths, consistent with the fact that the Spiro-TTB layer is mostly transparent in this region. The low reflectance of the samples in the UV region, between 300 and 400 nm, is due to the main absorption of Spiro-TTB and the decrease in

the reflectance of silver in the UV. In addition, when compared with the undoped Spiro-TTB film, the non-annealed doped film (Spiro-TTB:F6-TCNNQ) showed a small but clearly visible decrease in reflectance between 450 and 570 nm, which indicates a higher absorption of the non-annealed Spiro-TTB:F6-TCNNQ sample in this spectral region. This absorption feature has previously been attributed to the presence of a charge transfer (CT) state between Spiro-TTB and F6-TCNNQ.^[49]

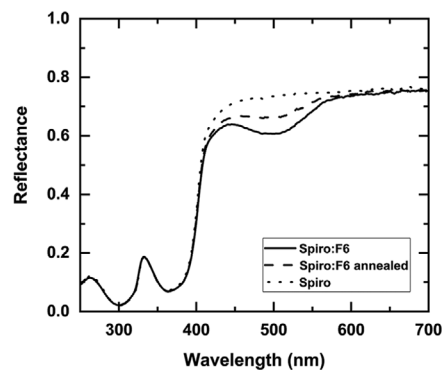


Figure 3. Reflectance spectra of 40 nm-thick films of Spiro-TTB on 80 nm-thick silver layers. Doped with F6-TCNNQ and non-annealed (Spiro:F6), doped with F6-TCNNQ and annealed at 80 °C for 6 h (Spiro:F6 annealed), and without F6-TCNNQ doping and non-annealed (Spiro). Samples were deposited on quartz substrates and reflectance was detected at an angle of incidence of 40°.

Therefore, our observation provides evidence of successful molecular p-doping in the non-annealed sample.

Comparing the reflection spectrum of the non-annealed doped film with the spectrum of an identical film that was annealed at 80 °C for 6 h, we find that after annealing the reflection in the CT state region increases, that is, the absorption decreases. There were no significant differences between the two samples in other regions of the spectrum. Generally, each dopant molecule can donate at most one charge to the surrounding material, resulting in a maximum doping efficiency of 100%.^[50] However, in practice the equilibrium ionization efficiency is often well below unity and will be reduced by any parasitic reaction of dopant molecules. We interpreted the decrease in CT absorption after annealing as a reduction in doping efficiency due to diffusion of silver into the HTL, possibly caused by a reaction of silver with the relatively unstable F6-TCNNQ. A reduction in doping efficiency has immediate impact on the electrical properties of the HTL, both in terms of hole injection from the anode and for hole-transport to the emissive layer. This reduction can thus explain the very large decrease in current density and luminance of top-emitting OLEDs during ALD encapsulation.

2.4. Thermal Stability and Lifetime of Improved Organic Light-Emitting Diodes

Above we have shown that avoiding the use of F6-TCNNQ or replacing F6-TCNNQ with MoO₃ provides good thermal stability of the interface between the silver anode and the HTL. We therefore attempted to make ALD encapsulated top-emitting OLEDs in which F6-TCNNQ p-doping is replaced entirely with MoO₃. While these devices showed similar performance for glass and ALD encapsulation, their luminance at 5 V was threefold lower than for glass-encapsulated OLEDs using F6-TCNNQ, with the performance decreasing further with increasing MoO₃ doping (Figure S6, Supporting Information).

We concluded that a threefold drop in luminance will not be acceptable for most applications and thus that the use of an efficient molecular p-dopant like F6-TCNNQ is necessary. This is particularly important when a thick HTL is needed, for example, to achieve operation of devices in the 2nd order optical cavity mode. To stabilize the silver/HTL interface without sacrificing the use of F6-TCNNQ, we either inserted an ultrathin MoO₃

buffer layer (i.e., Ag/MoO₃/Spiro-TTB:F6-TCNNQ) or used a bilayer HTL (i.e., Ag/Spiro-TTB:MoO₃/Spiro-TTB:F6-TCNNQ). We also screened a range of thickness ratios between the two sublayers of the bilayer HTL while keeping the total thickness of the bilayer HTL fixed. Further information on the buffer layer structure and the bilayer structure as well as on the current density, luminance, and EQE that devices based on them achieved is summarized in Table 1.

Figure 4a,b shows the *j*V and EQE characteristics of these top-emitting OLEDs, encapsulated again either with a conventional cover glass or by using the ALD process at 80 °C. In the original device with the immediate silver/p-HTL interface (reference), the current density at 5 V dropped from 310 to 60 mA cm⁻² and the luminance decreased from 11 000 to 2900 cd m⁻² after ALD encapsulation. By contrast, device degradation was significantly reduced in all revised structures. The OLED with the ultrathin MoO₃ buffer layer even exhibited improved hole injection over the original device when using glass encapsulation and showed only a relatively minor loss in current density and luminance upon ALD encapsulation. The resilience to ALD encapsulation was also greatly enhanced for devices using bilayer HTLs. However, the current density and EQE both gradually decreased with increasing thickness of the MoO₃-doped sublayer (Table 1). This is consistent with the relatively low current density we previously observed in the MoO₃-based p-i-p device and complete OLEDs that exclusively used MoO₃ doping. In addition to retaining high current density and luminance at 5 V, the revised structures showed reduced leakage current and increased EQE when encapsulated with ALD versus conventional glass encapsulation. We attribute the reduction in leakage current to morphological changes during the extended heating to 80 °C. The increase in EQE is an indirect effect of the reduced leakage and may further be a result of improved light outcoupling efficiency due to changes in micro-cavity optics. This latter hypothesis is supported by the fact that ALD encapsulation slightly changed the electroluminescence spectra of the different OLEDs (Figure 4c).

Apart from the blue top-emitting OLEDs presented so far, we have also successfully used 1,4,5,8,9,11-hexaazatriphenylene hexacarbonitrile (HAT-CN) as an alternative buffer layer to MoO₃ in top-emitting blue OLEDs (Figure S7, Supporting Information). In addition, we verified our ultrathin buffer layer concept for phosphorescent red top-emitting OLEDs and for blue bottom-emitting OLEDs with a thin silver bottom contact

Table 1. Summary of the different HTL compositions tested, as well as the current density, luminance, and EQE at 5 V reached by top-emitting OLEDs using these HTL compositions when encapsulating OLEDs with either a cover glass or ALD. The values listed are the average of eight pixels within one device.

| | Current density at 5 V [mA cm ⁻²] | | Luminance at 5 V [cd cm ⁻²] | | EQE at 5 V [%] | |
|--|---|-----|---|-------|----------------|------|
| | Glass | ALD | Glass | ALD | Glass | ALD |
| Reference Spiro:F6 [150 nm] | 312 | 56 | 10 966 | 2887 | 2.21 | 2.74 |
| MoO ₃ [1 nm]/Spiro:F6 [150 nm] | 345 | 263 | 11 807 | 10551 | 1.99 | 2.05 |
| Spiro:MoO ₃ /Spiro:F6 [5/145 nm] | 290 | 202 | 8587 | 7241 | 1.97 | 2.32 |
| Spiro:MoO ₃ /Spiro:F6 [10/140 nm] | 289 | 201 | 7817 | 7276 | 1.93 | 2.26 |
| Spiro:MoO ₃ /Spiro:F6 [20/130 nm] | 243 | 180 | 7771 | 6462 | 1.82 | 2.20 |
| Spiro:MoO ₃ /Spiro:F6 [40/110 nm] | 237 | 159 | 7530 | 5844 | 1.74 | 2.00 |

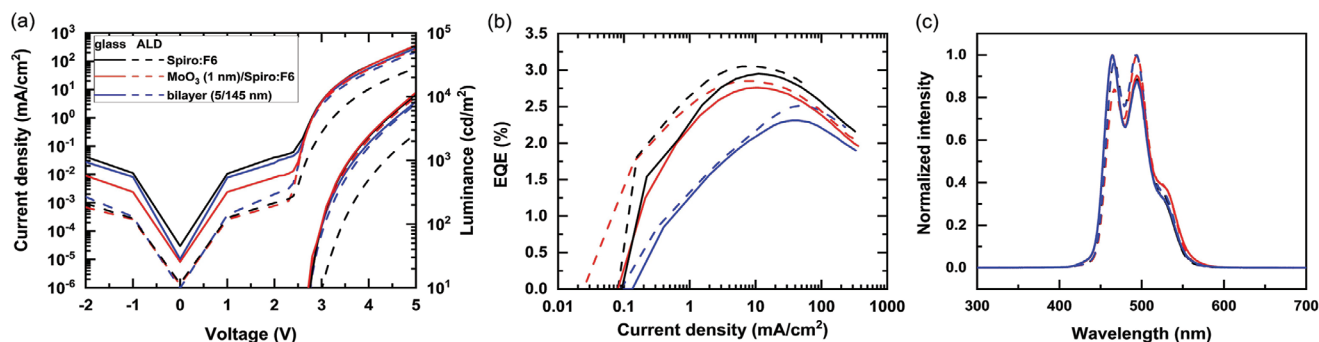


Figure 4. a) j/VL characteristics of top-emitting OLEDs with glass and ALD encapsulation and with different HTLs; Spiro-TTB doped with F6-TCNNQ as in Figure 1 (Spiro:F6), an ultrathin buffer layer at the silver/HTL interface (MoO₃ (1 nm)/Spiro:F6), and a bilayer HTL with 5 nm-thick MoO₃ doped Spiro-TTB layer and 145 nm-thick F6-TCNNQ doped Spiro-TTB layer (bilayer (5/145 nm)). b) EQE versus current density for the same devices as in (a). c) Normalized electroluminescence spectra for the same devices as in (a).

(Figure S8, Supporting Information). As expected, devices with the buffer layer showed similar j/VL characteristics for glass and ALD encapsulation, while a large reduction in current density and luminance upon ALD encapsulation was observed in devices without buffer layer.

Finally, we tested the operational lifetime of top-emitting OLEDs with and without an ultrathin buffer layer of MoO₃ using a constant current driving scheme. For devices with the buffer layer, there was no substantial difference in device lifetime between glass and ALD encapsulation (Figure S9, Supporting Information). For simplicity, the following comparison was therefore performed with conventional glass encapsulation. Figure 5a summarizes the lifetime of OLEDs with and without buffer layer for different initial luminance values. Here, lifetime was defined as the time under continuous constant current driving until the luminance decreased to 65% of L_0 . At $L_0 = 4000$ cd m⁻², the device without MoO₃ buffer layer showed a slightly longer lifetime ($\tau_{65\%} = 87$ h) than the device with MoO₃ buffer layer (64 h). At $L_0 = 8000$ cd m⁻², this difference decreased to just 3.7 h and a crossover occurred when the initial luminance was increased further to 15 000 cd m⁻². At the highest initial luminance tested here

($L_0 = 30\,000$ cd m⁻²), the device with MoO₃ buffer layer exhibited 28% longer lifetime than the OLED with the direct silver Spiro-TTB:F6-TCNNQ interface.

The data in Figure 5a was then fitted to $\tau_{65\%} = \log L_0^{-\beta}$, where β is the acceleration factor.^[51] For OLEDs without buffer layer, the acceleration factor was $\beta_1 = 2.32$, larger than for devices with buffer layer where $\beta_2 = 2.03$. This difference in acceleration factor again reflects the fact that the MoO₃ buffer layer prevents device degradation at high luminance levels.

The difference between OLEDs with and without buffer layer becomes even more pronounced when devices are operated beyond their $\tau_{65\%}$ time (Figure 5b). At $L_0 = 30\,000$ cd m⁻² the OLED without buffer layer dropped to less than 20% of its initial luminance after 2.5 h while the device with buffer layer remained at over 20% of L_0 until the end of the test after 5 h. The complete luminance decay curves for all tested conditions are provided in Figure S10, Supporting Information.

We attribute the improved lifetime of OLEDs with MoO₃ buffer layer under operation at high luminance to the fact that the devices heat up under these driving conditions. As for the ALD encapsulation, this heating causes degradation of the silver/HTL interface if the F6-TCNNQ doped film is in direct

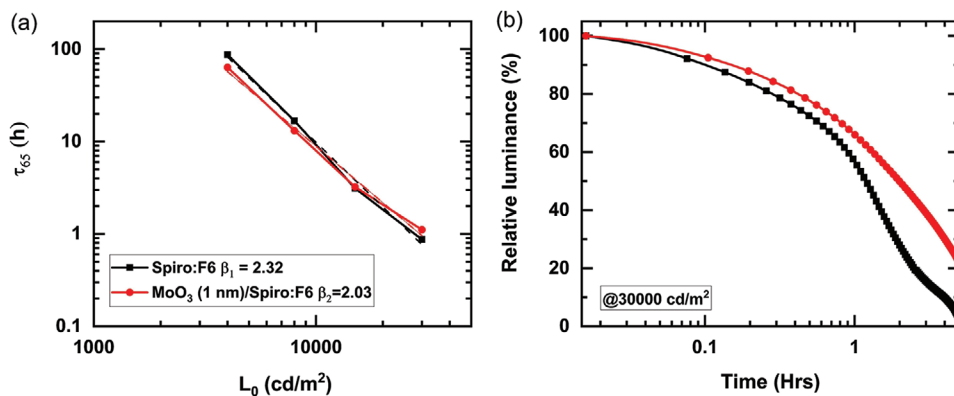


Figure 5. a) Comparison of device lifetime τ_{65} for top-emitting OLEDs with an F6-TCNNQ doped HTL directly deposited on the silver anode (Spiro:F6) and with ultrathin MoO₃ buffer layer inserted between silver and HTL (MoO₃ (1 nm)/Spiro:F6). Devices were driven at the current required to reach a set of different initial luminance levels L_0 . The dashed lines represent fits to the data to determine the acceleration factor β for each OLED structure. b) The relative luminance of top-emitting OLEDs with (red circles) and without (black squares) ultrathin MoO₃ buffer layer over time under constant current drive and for an initial luminance level of 30 000 cd m⁻².

contact with silver. By contrast, the presence of a thin buffer layer, prevents heat-induced degradation of the surface and thus reduces device degradation.

3. Conclusion

In conclusion, we investigated the degradation in current density and luminance in top-emitting OLEDs upon encapsulation with a low temperature ALD process. To understand the underlying mechanism, single charge carrier devices were investigated, and it was found that the interface between the bottom silver electrode and p-HTL was the main cause for the decrease in current density and luminance. The interaction between the diffusing silver ions and the p-dopant F6-TCNNQ at elevated temperatures was identified as the likely origin of this effect by a spectroscopic study of thin films. To stabilize the interface, we either inserted an ultrathin buffer layer of MoO₃ or used a bilayer HTL, with both approaches effectively inhibiting device degradation during ALD encapsulation. Finally, we performed studies of device lifetime and found that inserting an ultrathin MoO₃ buffer layer also delays device degradation at high luminance levels.

The top-emitting configuration of OLEDs is preferable in terms of fill factor and aperture ratio in various practical applications. We believe that our work provides an effective solution to the problem of temperature induced degradation of top-emitting p-i-n OLEDs without introducing significant additional complexity to the fabrication process. This is relevant not only to encapsulation by ALD, but to any post-processing step that requires elevated temperature. As such, this study paves the way for new applications of top-emitting OLEDs, in particular with regards to integration on silicon/CMOS driver chips, as required for use in augmented reality and virtual reality applications and biosensing.

4. Experimental Section

Organic Light-Emitting Diodes Fabrication: Display grade glass substrates (Eagle XG, Corning) were cleaned with acetone and isopropyl alcohol in an ultrasonic bath. OLEDs were deposited in a high-vacuum thermal evaporator chamber (EvoVac, Angstrom Engineering Inc.) with a base pressure of 10⁻⁷ mbar. Using custom made shadow masks (LiMaB GmbH) for the anode, organic, and cathode layers, pixels with an active area of 2 × 2 mm² were defined. The starting device structure used in this study was as follows: Ag (80 nm)/Spiro-TTB:F6-TCNNQ (4 wt%)/N,N'-di(naphthalene-1-yl)-N,N'-diphenylbenzidine (NPB)/2-methyl-9,10-bis(naphthalen-2-yl)anthracene (MADN):2,5,8,11-tetra-tert-butylperylene (TBPe) (1.5 wt%)/bis-(2-methyl-8-chinolinolato)-(4-phenyl-phenolato)-aluminum(III) (BALq)/BPhen:Cs (3 wt%)/Ag (20 nm)/NPB (40 nm). Here, Spiro-TTB was doped with F6-TCNNQ dimalononitrile as the HTL. The blue fluorescent emitter TBPe was doped into the host MADN as the light-emitting layer. BPhen was co-evaporated with pure Cs metal to form the ETL. NPB and BALq were used as the electron blocking layer and hole blocking layer, respectively. NBPhen and TPBi were used as alternative ETL materials. Molybdenum trioxide (MoO₃) was used as alternative p-type dopant and as buffer layer. HAT-CN was also tested as buffer layer. For red top-emitting OLEDs, (2-methylidibenzo[f,h]quinoxaline)(acetylacetonate)iridium(III) was doped into NPB at 10 wt% as the EML. All organic materials were purchased from Lumtec and LG Chem.

Atomic Layer Deposition Encapsulation: ALD encapsulation was applied similar to the procedure described in ref. [38]. In brief, alternating layers of Al₂O₃ and ZrO₂, each with a nominal thickness

of 3 nm, were deposited up to a total thickness of 150 nm. For Al₂O₃, trimethylaluminum (TMA) and H₂O were used as precursors with each precursor being pulsed for 15 ms with 10 s purging intervals of N₂ in between. For ZrO₂, tetrakis(dimethylamino)zirconium (TDMAZr) and H₂O were used as precursors, with TDMAZr pulsed for 0.3 s and H₂O pulsed for 30 ms and with 7 s purging intervals of N₂ in between pulses. The working temperature for the TDMAZr cylinder was 75 °C, while the TMA and H₂O precursors were maintained at room temperature. The temperature of the ALD chamber (Savannah S200, Ultratech) was 80 °C, and the chamber pressure was ≈0.21 Torr.

Device Characterization: jV characteristics of single charge carrier devices (n-i-n and p-i-p devices) were measured by a source measurement unit (2400 SourceMeter, Keithley Instruments). jVL characteristics of OLEDs were measured with the same SourceMeter and a calibrated silicon photodiode. Electroluminescence spectra were measured by a spectrograph (MS125, Oriel) coupled to a CCD camera (DV420-BU, Andor). EQE was calculated assuming a Lambertian emission profile. The lifetime of OLEDs was measured by monitoring the relative luminance decay over time at constant current driving using a commercial lifetime testing system (M6000, McScience). Device characterization was carried out at room temperature under ambient conditions.

Thin-Film Characterization: 40 nm-thick doped HTLs (Spiro-TTB:F6-TCNNQ (4 wt%)) and undoped HTLs (Spiro-TTB) were deposited on top of 80 nm-thick Ag layers on quartz substrates using the same evaporation chamber as for OLED fabrication. For annealing, samples were transferred to the ALD reactor immediately after preparation and kept at a temperature of 80 °C for 6 h without performing any ALD cycles. The spectral reflectance was measured using an ellipsometer (M-2000, J. A. Woollam).

Supporting Information

Supporting Information is available from the Wiley Online Library or from the author. The research data supporting this publication can be accessed at <https://doi.org/10.17630/5b353f82-dbe5-4926-afb0-85e1a9373686>.

Acknowledgements

This research was financially supported by the EPSRC NSF-CBET lead agency agreement (EP/R010595/1, 1706207), the DARPA-NESD program (N66001-17-C-4012), and the Leverhulme Trust (RPG-2017-231). Y.D. acknowledges a stipend from the Chinese Scholarship Council (CSC). C.K. acknowledges support from the Basic Science Research Program through the National Research Foundation of Korea (NRF) funded by the Ministry of Education (2017R1A6A3A03012331). M.C.G. acknowledges support from the Alexander von Humboldt Stiftung through the Humboldt-Professorship.

Conflict of Interest

The authors declare no conflict of interest.

Keywords

atomic layer deposition encapsulation, buffer layer, device degradation, silver diffusion, thermal stability, top-emitting organic light-emitting diodes

Received: September 22, 2020

Revised: October 27, 2020

Published online:

- [1] H.-W. Chen, J.-H. Lee, B.-Y. Lin, S. Chen, S.-T. Wu, *Light: Sci. Appl.* **2018**, *7*, 17168.
- [2] N. Thejo Kalyani, S. J. Dhoble, *Renewable Sustainable Energy Rev.* **2012**, *16*, 2696.
- [3] S. Hofmann, M. Thomschke, B. Lüssem, K. Leo, *Opt. Express* **2011**, *19*, S6.
- [4] S. Chen, L. Deng, J. Xie, L. Peng, L. Xie, Q. Fan, W. Huang, *Adv. Mater.* **2010**, *22*, 5227.
- [5] F. Templier, *OLED Microdisplays: Technology and Applications*, John Wiley & Sons, New York **2014**.
- [6] A. Buckley, I. Underwood, C. J. Yates, in *Organic Light-Emitting Diodes (OLEDs)*, (Ed: A. Buckley), Woodhead Publishing, Cambridge **2013**, pp. 459–511.
- [7] F. Ventsch, M. C. Gather, K. Meerholz, *Org. Electron.* **2010**, *11*, 57.
- [8] A. Steude, M. Jahnel, M. Thomschke, M. Schober, M. C. Gather, *Adv. Mater.* **2015**, *27*, 7657.
- [9] A. Steude, E. C. Witts, G. B. Miles, M. C. Gather, *Sci. Adv.* **2016**, *2*, e1600061.
- [10] W. Cao, J. Li, H. Chen, J. Xue, *J. Photonics Energy* **2014**, *4*, 040990.
- [11] T. Schwab, S. Schubert, L. Müller-Meskamp, K. Leo, M. C. Gather, *Adv. Opt. Mater.* **2013**, *1*, 921.
- [12] S. D. Yambem, M. Ullah, K. Tandy, P. L. Burn, E. B. Namdas, *Laser Photonics Rev.* **2014**, *8*, 165.
- [13] N. Sun, G. Fang, H. Xiao, J. Li, Q. Zheng, M. Wang, N. Liu, X. Zhao, J. Liu, D. L. Carroll, *2009 Symp. on Photonics and Optoelectronics*, IEEE eXpress Conference Publishing, Wuhan **2009**.
- [14] T. Dobbertin, M. Kroeger, D. Heithecker, D. Schneider, D. Metzendorf, H. Neuner, E. Becker, H.-H. Johannes, W. Kowalsky, *Appl. Phys. Lett.* **2003**, *82*, 284.
- [15] Y.-M. Chien, F. Lefevre, I. Shih, R. Izquierdo, *Nanotechnology* **2010**, *21*, 134020.
- [16] P. Freitag, Al. A. Zakhidov, B. Luessem, A. A. Zakhidov, K. Leo, *J. Appl. Phys.* **2012**, *112*, 114505.
- [17] P. Freitag, S. Reineke, S. Olthof, M. Furno, B. Lüssem, K. Leo, *Org. Electron.* **2010**, *11*, 1676.
- [18] C.-W. Chen, P.-Y. Hsieh, H.-H. Chiang, C.-L. Lin, H.-M. Wu, C.-C. Wu, *Appl. Phys. Lett.* **2003**, *83*, 5127.
- [19] M. Qian, X.-B. Shi, J. Ma, J. Liang, Y. Liu, Z.-K. Wang, L.-S. Liao, *RSC Adv.* **2015**, *5*, 96478.
- [20] C. Dong, X. Fu, S. Amoah, A. Rozelle, D. H. Shin, A. Salehi, F. So, *J. Soc. Inf. Disp.* **2019**, *27*, 469.
- [21] M. C. Gather, S. Reineke, *J. Photonics Energy* **2015**, *5*, 057607.
- [22] S. Hofmann, M. Thomschke, P. Freitag, M. Furno, B. Lüssem, K. Leo, *Appl. Phys. Lett.* **2010**, *97*, 253308.
- [23] G. He, O. Schneider, D. Qin, X. Zhou, M. Pfeiffer, K. Leo, *J. Appl. Phys.* **2004**, *95*, 5773.
- [24] B. Lüssem, M. Riede, K. Leo, *Phys. Status Solidi A* **2013**, *210*, 9.
- [25] S. Scholz, D. Kondakov, B. Lüssem, K. Leo, *Chem. Rev.* **2015**, *115*, 8449.
- [26] Y. H. Choi, Y. P. Jeon, D. C. Choo, T. W. Kim, *Org. Electron.* **2015**, *22*, 197.
- [27] T. Maindron, J.-Y. Simon, E. Viasnoff, D. Lafond, *Thin Solid Films* **2012**, *520*, 6876.
- [28] F. A. Angel, J. U. Wallace, C. W. Tang, *Org. Electron.* **2017**, *42*, 102.
- [29] P. Philipp, K. Q. Ngo, J. Kieffer, T. Wirtz, *J. Phys. Chem. C* **2015**, *119*, 23334.
- [30] W.-C. Lin, W.-B. Wang, Y.-C. Lin, B.-Y. Yu, Y.-Y. Chen, M.-F. Hsu, J.-H. Jou, J.-J. Shyue, *Org. Electron.* **2009**, *10*, 581.
- [31] D. Spee, K. van der Werf, J. Rath, R. Schropp, *Phys. Status Solidi RRL* **2012**, *6*, 151.
- [32] D. Yu, Y.-Q. Yang, Z. Chen, Y. Tao, Y.-F. Liu, *Opt. Commun.* **2016**, *362*, 43.
- [33] J. Meyer, P. Görrn, F. Bertram, S. Hamwi, T. Winkler, H.-H. Johannes, T. Weimann, P. Hinze, T. Riedl, W. Kowalsky, *Adv. Mater.* **2009**, *21*, 1845.
- [34] J.-S. Park, H. Chae, H. K. Chung, S. I. Lee, *Semicond. Sci. Technol.* **2011**, *26*, 034001.
- [35] Q. Huang, K. Walzer, M. Pfeiffer, K. Leo, M. Hofmann, T. Stübinger, *J. Appl. Phys.* **2006**, *100*, 064507.
- [36] S. Naka, H. Okada, H. Onnagawa, T. Tsutsui, *Appl. Phys. Lett.* **2000**, *76*, 197.
- [37] J.-H. Lee, M.-H. Wu, C.-C. Chao, H.-L. Chen, M.-K. Leung, *Chem. Phys. Lett.* **2005**, *416*, 234.
- [38] C.-M. Keum, N. M. Kronenberg, C. Murawski, K. Yoshida, Y. Deng, C. Berz, W. Li, M. Wei, I. D. W. Samuel, M. C. Gather, *Adv. Opt. Mater.* **2018**, *6*, 1800496.
- [39] F. Steuber, J. Staudigel, M. Stössel, J. Simmerer, A. Winnacker, H. Spreitzer, F. Weissörtel, J. Salbeck, *Adv. Mater.* **2000**, *12*, 130.
- [40] S. Tokito, H. Tanaka, K. Noda, A. Okada, Y. Taga, *Appl. Phys. Lett.* **1997**, *70*, 1929.
- [41] F. Zhang, A. Kahn, *Adv. Funct. Mater.* **2018**, *28*, 1703780.
- [42] S. Gao, C. Song, C. Chen, F. Zeng, F. Pan, *Appl. Phys. Lett.* **2013**, *102*, 141606.
- [43] M. Lauters, B. McCarthy, D. Sarid, G. E. Jabbour, *Appl. Phys. Lett.* **2005**, *87*, 231105.
- [44] Y. Yang, P. Gao, S. Gaba, T. Chang, X. Pan, W. Lu, *Nat. Commun.* **2012**, *3*, 732.
- [45] A. A. Grinberg, S. Luryi, *J. Appl. Phys.* **1987**, *61*, 1181.
- [46] X. Haitao, Z. Xiang, *J. Appl. Phys.* **2013**, *114*, 244505.
- [47] Q. Y. Bao, J. P. Yang, Y. Q. Li, J. X. Tang, *Appl. Phys. Lett.* **2010**, *97*, 063303.
- [48] M. Kröger, S. Hamwi, J. Meyer, T. Riedl, W. Kowalsky, A. Kahn, *Org. Electron.* **2009**, *10*, 932.
- [49] C. Murawski, C. Fuchs, S. Hofmann, K. Leo, M. C. Gather, *Appl. Phys. Lett.* **2014**, *105*, 113303.
- [50] D. Kiefer, R. Kroon, A. I. Hofmann, H. Sun, X. Liu, A. Giovannitti, D. Stegerer, A. Cano, J. Hynynen, L. Yu, Y. Zhang, D. Nai, T. F. Harrelson, M. Sommer, A. J. Moulé, M. Kemerink, S. R. Marder, I. McCulloch, M. Fahlman, S. Fabiano, C. Müller, *Nat. Mater.* **2019**, *18*, 149.
- [51] A. R. Buckley, C. J. Yates, I. Underwood, *J. Soc. Inf. Disp.* **2009**, *17*, 611.